



In silico investigation on the twisting of gold nanowires

Guangyu He^a, Ruoxu Wang^b, Jie Fan^c, Shi Liu^b, Hongyu Chen^{b,*}

^a Research Institute of Zhejiang University-Taizhou, Taizhou 318000, Zhejiang Province, China

^b School of Science, Westlake University, 18 Shilongshan Road, Hangzhou 310024, Zhejiang Province, China

^c Department of Chemistry, Zhejiang University, Hangzhou 310027, China

ARTICLE INFO

Keywords:

Stochastic surface walking
Neural network potential
Nanowire
Twisting
Chirality

ABSTRACT

Ultrathin Au and Au alloy nanowires upon coating of a metal layer are known to twist, and such twisting is of importance for driving motions in minuscule systems. Here, with global exploration of potential energy surface, the origin of twisting Au nanowire is investigated. Au nanowire with Face Center Cubic structure would transform into a helix with multi-shell atomic structure, driven by general increase of effective bonding (thermodynamics), where the largest contribution comes from the surface atoms. On the other hand, the rectangular nanowire comes out with Boerdijk–Coxeter–Bernal like structure. Studies on the progresses of transformations indicate that it is composed of local bending which leads to twisting of nanowire. It is conceivable that the understanding of such systems would shed light to future synthetic designs of twisting nanowires and for introducing chirality into nanowires.

1. Introduction

Mechanical motion driven by energy conversion is very common in our daily life, such as the conversion of chemical energy in steam engines, combustion engines and the conversion of electric energy in electric motors. Historically, it is also the critical point of breakthrough in the industry revolution. Thus, it is conceivable that similar concepts at the nanoscale are of great significance to the development of nanotechnology.

In contrast to engines and motors, the energy conversion in minuscule systems could often directly drive motion or shape transformation, enabling unique capabilities. For example, floating particles or little boats on water surface could be driven by the Marangoni effect of surfactants; [1] and a magnetic helix could be driven by external magnetic field to deliver a sperm to an egg cell [2].

It has been shown that the contraction of polymer micelles or emulsion droplets could compress nanowires or nanotubes into ring structures, converting the surface energy into the stored mechanical energy [3–5]. More interestingly, ultrathin metal nanowires upon coating with atomic layers of metal could be twisted into double helices [6,7] or weaved into nanoropes [8], where the chemical energy drives the morphological transformation.

With the development of in situ characterization tool, it has been an important approach to observe the progress in nanoscale directly.

Recently, an in situ atomic-resolution study is conducted to track time-resolved, atomic-scale motion of grain boundary, and observes some unreported sliding of general tilt boundaries [9]. Also, bending of Ag nanowire with homemade deformation device is found to cause the phase transition from face-centered cubic to body-centered cubic and hexagonal-close packed with in situ investigations which reveals a new deformation mechanism of nanowires under bending strain [10]. Hence, the spontaneous twisting of nanowire, a similar progress should also have unique lattice transformation. Unfortunately, while mechanisms have been postulated about the twisting of nanowires and the weaving of nanoropes [8], in-depth investigation has been hampered by the instability of the ultrathin nanowires under electron beam bombardment.

Computational simulation is another suitable way to investigate such progress. In terms of general nanowire studies, phase transformations [11–13] and their reversibility correlated to shape memory [14–16] have been investigated with Molecular Dynamics (MD) simulations, which could reveal atomic details. The attention is on the shortening and extension of nanowires at the axial direction, and there is little mentioning of nanowire twisting behavior nor the underlying mechanism which may be ascribed to the size of investigated nanowires [17]. The global search on the lattice transformation of nanowires is tough with common MD simulations as well.

In this work, with the aid of neural network potential energy surface and stochastic surface walking algorithm, we study the intrinsic twisting

* Corresponding author.

E-mail address: chenhongyu@westlake.edu.cn (H. Chen).

<https://doi.org/10.1016/j.mtcomm.2022.104319>

Received 4 July 2022; Received in revised form 22 August 2022; Accepted 24 August 2022

Available online 31 August 2022

2352-4928/© 2022 Elsevier Ltd. All rights reserved.

behavior of Au nanowires. The structural transformation of Au nanowires with Face Center Cubic (FCC) lattice structure is investigated and the transformation to helical nanowires should be caused by twisting composed of local bending. Studies on the atomic stability with different coordination numbers reveal that the transformation is mainly driven by the improved bonding for the low-coordination edge atoms (from 5- to 7- and 8-coordination), at the cost of the internal atoms (from the most stable 12- to 9–11-coordination). Transformations of Au nanowires with different initial morphology show that all structures are moving towards the multi-shell structure, though the kinetic pathways are often locked at the intermediate meta-stable states. We believe that the findings in this work would provide a new perspective on nanowire transformation, revealing the atomic details of the chiral nanowires and quantitative understanding of the driving force and the kinetic barriers.

2. Methods

All simulations based on neural network potential are carried out by using Large-scale Atomic Simulation with neural network Potential (LASP, www.lasphub.com) software [18]. SSW-NN method [19] is used for fast global structure search which implements the stochastic surface walking (SSW) global optimization [20] based on Cu-Ag-Au global neural network (NN) potential [21] provided in Global Neural Network potential Library (<http://www.lasphub.com/#/lasphub/nnLibrary>). The method is demonstrated to be successful in a number of solid materials [22,23] and organic molecules [24]. The SSW algorithm is a global optimization method which is developed to explore both minima and saddle points on potential energy surface (PES) without any pre-determined guess. It can manipulate a structural configuration moving smoothly from a local minimum to a high-energy configuration along one random mode direction by sequentially added bias Gaussian potential. The NN potential is generated by iterative self-learning of the density functional theory (DFT) global PES data set generated from SSW exploration which covers a wide range of different structural types (bulks, surfaces and clusters) until the NN potential is transferable and robust enough to describe the global PES. In total, a training dataset consists of 37223 structures are selected to represent the global PES and the high-accuracy DFT calculations are implemented in Vienna Ab-initio Simulation Package (VASP) [25]. The DFT functional is at the level of the generalized gradient approximation (GGA) with the Perdew–Burke–Ernzerhof functional (PBE) [26]. The kinetic energy cutoff is 450 eV, and the projector augmented wave (PAW) pseudopotential [27] is utilized to describe ionic core electrons. The first Brillouin zone k-point sampling utilizes the Monkhorst–Pack scheme with an automated mesh determined by 25 times the reciprocal lattice vectors [28]. To build the NN potential, each elementary network (Cu, Ag, and Au) contains 205 input neurons from different types of power-type structural descriptors, associated with two hidden layers each with 50 neurons. For the final NN potential, the root mean square (RMS) errors for the energy and force were 3.59 meV/atom and 0.04 eV/Å, respectively, which would come up with reliable results (more details are presented in [supporting information](#)). We have benchmarked the NN calculations against DFT results for the low-Miller-index planes of Au, (100), (110) and (111), as well as the lattice transformation on Au(100) with Au atoms adsorbed, which shows that the NN potential is reliable for the calculations on Au ([Fig. S1](#), [Table S1](#) and [S2](#)). The DFT calculations are implemented with Quantum-ESPRESSO package [29]. Periodic boundary conditions are employed during the calculations. The GGA exchange-correlation functional proposed by PBE is employed. Electron-ion interactions are described using PAW (more details are presented in [supporting information](#)).

On the basis of global structure search by SSW-NN method, pathway building and transition state (TS) determination are completed via the double-ended surface walking (DESW) [30] in LASP. In the progress, the adjacent coordinates searched by SSW-NN method are set as the initial state (IS) and final state (FS). The TS are further confirmed by

extrapolation optimization to the correct IS and FS.

To get the coordination number of each Au atom, distances between any two Au atoms are calculated and 1.1 times of the bond length in Au crystal (2.88 Å) is set as the upper-limit of bonding.

Interactions between atoms with different coordination number and other atoms in nanowires are roughly estimated by dividing nanowire (structure 1) into a row of atoms (structure 3) and nanowire without a row of atoms (structure 2) to compare the energies ([Scheme 1](#)). Interactions are calculated through

$$E_{\text{interaction}} = E_{\text{structure1}} - E_{\text{structure2}} - E_{\text{structure3}}$$

Hexagonal nanowire (length: 40.97 Å) is studied for its regular structure as the atoms in the same row at axial direction have same coordination number. The rows investigated in this part is distinguished by the atoms' coordination number, and the atoms under different environments are taken into consideration.

As the rotation of atoms around the axis of nanowire have been postulated about the twisting in experiment, [8] the motion trails of atoms relative to the center axis in nanowire are obtained in following ways: the center axis of nanowire is set as the standard to calculate the relative displacements of atoms between adjacent structures in transformation. The rotation angles are calculated through

$$\theta = \cos^{-1} \left(\frac{a^2 + b^2 - c^2}{2ab} \right)$$

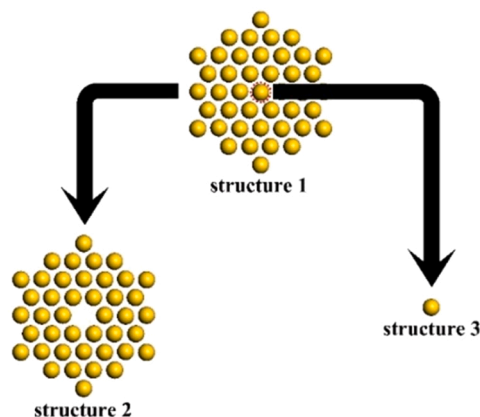
while a refers to the distance between initial site and the center axis of nanowire, b refers to the distance between final site and the center axis of nanowire, and c refers to the distance between initial site and final site on the projective plane at axial direction. Then, the direction of rotation is further verified by comparing the coordinates of initial and final sites. As we set the center axis of nanowire as the standard, it would introduce error when obvious twist takes place during the lattice transformation. Therefore, we mainly focus on the trajectories with smooth lattice transformation in this investigation.

3. Results and discussion

3.1. Overview of main findings

In this part, we first give an overview of the main findings. The transformations of different nanowires are shown in detail, and then we would discuss the origin of twisting.

With SSW algorithm, lattice transformations of FCC Au nanowires with different cross-sections are studied: The hexagonal nanowire ([Fig. 1A](#)) leaves the FCC starting-point and transforms into a helix with multi-shell atomic structure ([Fig. 1B](#)). During the progress, the nanowire undergoes complex motions which could be best described as a twisting



Scheme 1. Schematics illustrating the dividing of nanowire.

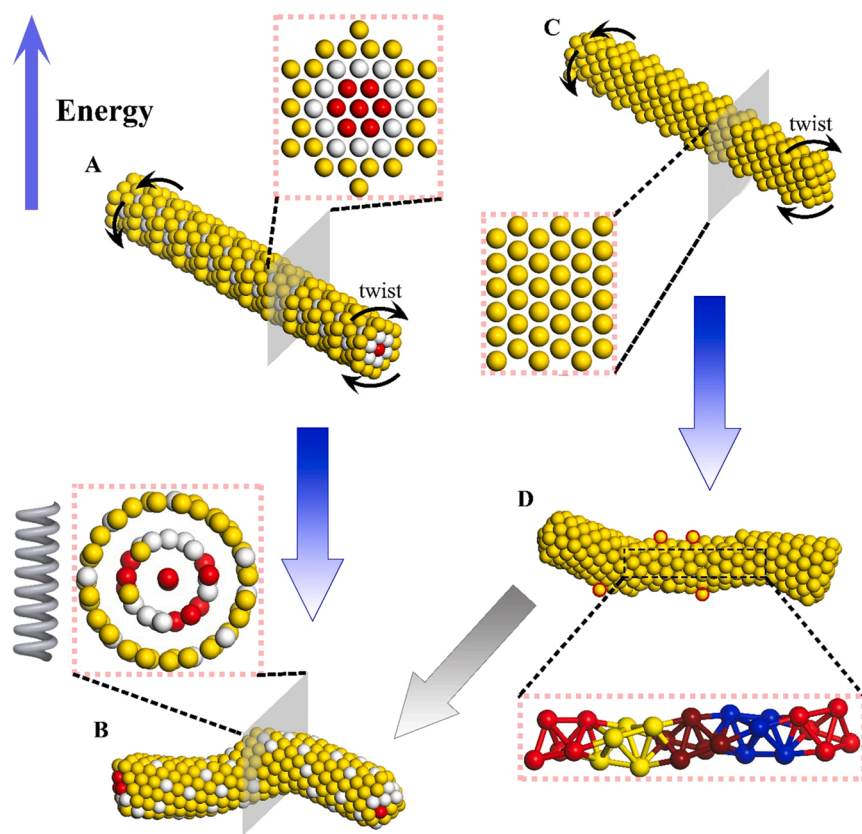


Fig. 1. Lattice transformation of FCC Au nanowires with different cross-sections. The relative height represents their respective energy. The atoms in A and B are marked with different colors to trace the atoms during the transformation, red for the innermost layer, yellow for the outermost layer, and white for the intermediate layer. Inner atoms in D are marked with different colors to help clarify the BCB structure. (For interpretation of the references to colour in this figure legend, the reader is referred to the web version of this article.)

of the two ends to the opposite directions. For the Au FCC nanowire with rectangular cross-section (Fig. 1C), it also leaves FCC starting-point and exhibits obvious twist. Fig. 1D shows a typical warped structure with close-packed surface atoms. The inner core of the warped nanowire is recognized to be the Boerdijk–Coxeter–Bernal (BCB) structure, which is essentially a chain of fused tetrahedra [31–33]. The stability of the BCB structure is evaluated by constructing a separate nanowire with pure BCB configuration, as opposed to the mere BCB core in the above case. After the transformation, part of the BCB feature is preserved, most notably the slant lines of surface atoms. From the cross-sectional view, an incomplete multi-shell characteristic could be recognized (Fig. 2C).

As summarized in Fig. 1, the multi-shell structure is the most favorable in energy among the 4 types of Au nanowires (hexagonal nanowire, rectangular nanowire, multi-shell structure and BCB structure), and the transformation pathways heavily rely on the initial nanowire structure. The most notable feature is that the staggered surface atoms of the FCC nanowires (Fig. 1A and C) turn into increasingly more close-packed arrangements (Fig. 1B and D), suggesting that the transformation is driven by the improved bonding among the surface atoms.

3.2. The computational models

More specifically, the starting hexagonal nanowire is set to have FCC lattice, with (111) planes perpendicular to the wire axis (Fig. 2A), on the basis of high-resolution transmission electron microscopy (HRTEM) study of the previous experimental work [6]. The side faces are in accordance with former investigations as well [34,35]. The diameter is 11.79 Å and the length is 79.41 Å, involving a total of 492 atoms. This diameter is similar as the lower end of the typical ultrathin nanowires (1.6 ± 0.4 nm) in the previous work [6]. With the constructed Au nanowire as the initial state, 64 independent SSW trajectories are run to explore the possible lattice transformations.

On the whole, most of the trajectories leave the FCC starting-point and transform into helices with a multi-shell atomic structure, with 7 of them show clear twisting. More specifically, 53 out of the 64 trajectories exhibit obvious bending and certain twisting, 4 trajectories transform into multi-shell atomic structure with slight bending, others keep FCC lattice at the middle part of nanowire which stay at the primary stage of transformation. With the breaking of FCC lattice, the atoms in each shell are slightly displaced, such that they form a tight helical arrangement around the central straight line of atoms. To trace the atoms during the complex transformation, the atoms in the initial nanowire are marked with different colors, red for the innermost layer, yellow for the outermost layer, and white for the intermediate layer (Fig. 1B). Due to the structural reorganization, a few atoms would inevitably move to adjacent layers, while the overall distributions are close to the initial locations. The multi-shell atomic structure is in accord with the Au nanowire prepared by electron beam etching, [36] where the 0.60 nm diameter measured in experiment corresponds to the inner shell of 0.54 nm diameter in our case. It is worth noting that the diameter of multi-shell atomic structure is 10.90 Å, thinner than the initial nanowire (11.79 Å).

To investigate the effects of morphology on the nanowire transformation, we construct Au FCC nanowire with rectangular cross-section (Fig. 2B, $7.21 \text{ Å} \times 9.16 \text{ Å}$; length: 68.29 Å; 360 atoms in total). Similar as the above case, the (111) planes are arranged in ABCABC... mode along the axial direction. Among the 64 independent SSW trajectories, most of them leave the FCC starting-point and exhibit obvious twist. More specifically, 57 trajectories out of the 64 trajectories exhibit obvious bending with 34 of them produce obvious twisting, 1 trajectory keeps FCC lattice at the middle part of nanowire which stays at the primary stage of transformation, others leave the FCC starting-point with slight bending. The twisted structures have distinct differences from the previous multi-shell atomic structures (Fig. 2A and B). It is noteworthy that a few atoms appear to have been squeezed out of the

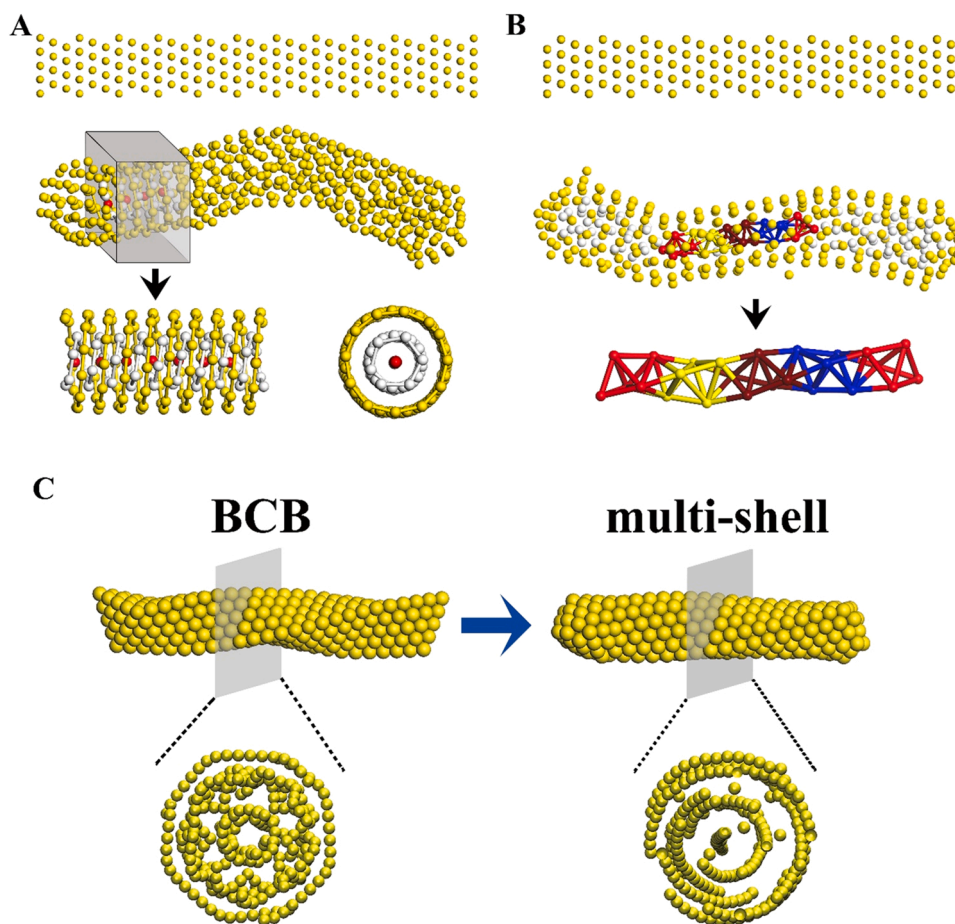


Fig. 2. The initial and the transformed structures of Au nanowires: (A) hexagonal nanowire, (B) rectangular nanowire, and (C) nanowire with BCB lattice structure.

nanowire forming isolated atoms on the surface (Fig. 1D, marked by red circles). Such atoms of low coordination number are expected to be quickly lost via dissolving or ripening in a real experiment. The inner core of the warped nanowire is recognized to be in accord with the BCB structure.

With concern for the relationship between multi-shell atomic structure and BCB structure, perfect BCB structure is constructed (Fig. 2C), where the high percentage of the Au(111) surface is expected to contribute favorably to the stability of the nanowire. The BCB type Au nanowire has a diameter of 11.43 Å and length of 68.13 Å, involving a total of 355 atoms. 64 independent SSW trajectories are run, and we focus on the trajectory with the most stable transformed structure. After the transformation, the acute dihedral angle of the constituent tetrahedra has disappeared in the product structure, where the surface atoms become more smooth and close-packed. It is well known that the high-curvature sites have a high surface energy owing to the lack of bonding partners. Thus, removing the sharp edges of the BCB nanowire should be a favorable factor. That is perhaps the reason that the real BCB nanowires all have rounded appearance [37]. From the cross-sectional view, an incomplete multi-shell characteristic (Fig. 2C) could be recognized as similar to that in Fig. 2A.

3.3. Energy diagram for the lattice transformation

By calculating the energy barriers in the trajectories with obvious twist, the channels with the lowest energy barriers for the hexagonal (Fig. 3A) and rectangular nanowires (Fig. 3B) are identified. The overall transformation of hexagonal nanowire is highly exothermic ($\Delta G = -37$ eV), which can be separated as three main stages of reorganization: The gentle initial decline involves the lattice damage at both ends of

nanowire. Then, the bending of left and right ends led to the first and second obvious steps, respectively. At last, the FCC lattice at the middle of nanowire is affected, corresponding to the third obvious step.

For the rectangular nanowire, its transformation is also exothermic with $\Delta G = -23$ eV. As shown in Fig. 3B, the breaking of lattice and bending at the right end led to the large decrease in energy. Then, a slight decrease corresponds to the change of lattice and bending at the left end. Finally, the lattice reorganization at the middle of nanowire completes the transformation from FCC to the BCB type nanowire.

For both cases, the lattice transformations are thermodynamically favorable, agreeing well with the qualitative assessment on the improvement of bonding for the surface atoms. The reorganization always starts at the ends, probably because the more exposed atoms there have a lower activation barrier towards structural changes, whereas the middle segment is more constrained. The largest energy barriers are only 0.76 and 0.68 eV for the two trajectories, so small that they are not obvious in the overall landscape. They also occur at the later stage and thus not critical for the overall structural transformation. It is worth noting that the main energy barrier for the rectangular nanowire before the first step is only 0.13 eV, which is much smaller than that of the hexagonal nanowire (0.37 eV). It explains the more rapid transformation for the rectangular nanowires among the various trajectories (Fig. S2, S3). These trajectories with low energy barriers suggest that the nanowires without ligand stabilization would leave FCC starting-point spontaneously, unlike the real nanowires with packed surface ligands.

In comparison, the transformation of the BCB nanowire is only slightly exothermic (Fig. 3C, $\Delta G = -8.43$ eV). The largest energy barrier at the initial stage is 0.67 eV which in general larger than those of the FCC nanowires (0.13 eV and 0.37 eV). Also, the relatively high energy barriers (0.82 eV, 0.89 eV, 0.85 eV and 0.90 eV) during the later-stage

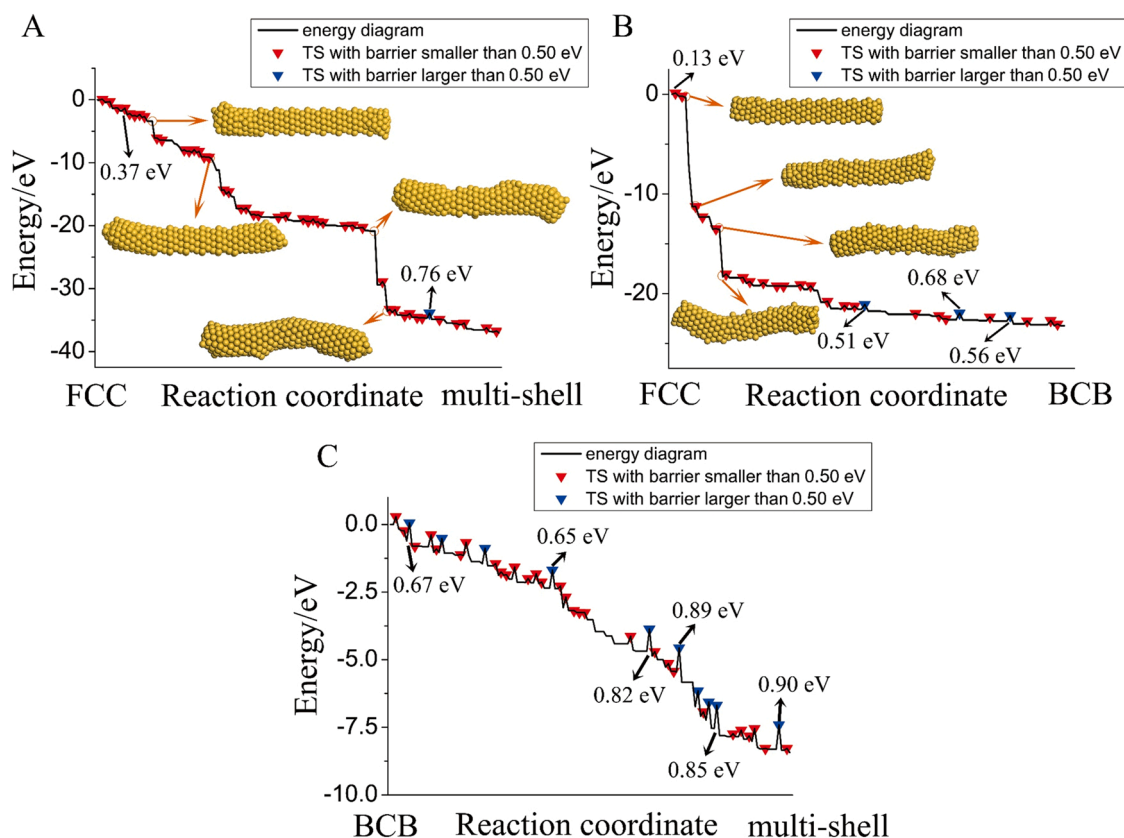


Fig. 3. Energy diagram for the lattice transformation of different Au nanowires: (A) hexagonal nanowire, (B) rectangular nanowire, and (C) nanowire with BCB lattice structure. Transition states (TS) with barrier smaller than 0.50 eV are marked by red inverted triangle, while the ones with barrier larger than 0.50 eV are marked by blue inverted triangle. The structures before and after the obvious energy decrease are given as illustrations. (For interpretation of the references to colour in this figure legend, the reader is referred to the web version of this article.)

transformation is probably the reason that the final product is locked at the stage of incomplete multi-shell structure.

For nanowires, FCC is clearly not the most stable lattice in terms of thermodynamics. The lack of neighboring atoms and insufficient bonding for the surface atoms are evident from the cross-sectional view and the surface topology (Figs. 1 and 2). Such exposed corners and edges of the FCC nanowires are clearly unstable, in contrast to the very stable FCC lattice in extended solids. Without ligand stabilization, there is a high tendency to leave the FCC lattice towards structures with more close-packed surface atoms. To this end, as the ideal FCC lattice cannot be compressed much (length for the nanowire) under mild environment, the structure undergoes a twist, which presumably stabilizes the surface atoms at the cost of the internal ones. In comparison, the initial nanowire structure with different cross-section and surface packing would affect the course of the transformation, resulting in various meta-stable structures, such as the BCB and the incomplete multi-shell structure.

3.4. Driving force for the lattice transformation

To gain a quantitative understanding of the driving force in transformation, we analyze the specific bonding situations for the FCC nanowires with different cross-sections, the BCB type nanowire, and the multi-shell type nanowire. The Au atoms are analyzed to obtain the average coordination number and bond lengths. Here, we define 3.17 Å as the upper-limit of effective bond, which is 1.1 times of the bond length in bulk Au crystal. As shown in Table 1, the average coordination number for the hexagonal nanowire is 8.67, and 8.07 for the multi-shell nanowire (multi-shell_FCC). More detailed breakdown is shown in the histogram (Fig. 4A), where the larger proportion of 12-coordination atoms is probably responsible for the larger average. On the other

Table 1
Average bonding numbers and average bonding lengths of atoms in FCC, BCB, multi-shell transformed from FCC and BCB.

	FCC	Multi-shell_FCC	Perfect BCB	BCB	multi-shell_BCB
$N_{\text{bonding_AVG}}$	8.67	8.07	8.79	7.83	7.85
Length_AVG/ Å	2.90	2.87	2.97	2.88	2.87

hand, the average bond length for the hexagonal nanowires (2.90 Å) is longer than the multi-shell nanowire (2.87 Å), suggesting that the latter has a higher quality of bonding. In other words, the FCC lattice is clearly favorable for the internal atoms with 12 bonds, but not for the overall nanowire, particularly considering the ultrathin diameter with dominant surface atoms. Basically, the multi-shell type nanowire strikes a balance between the surface and internal atoms (Fig. 4A, C). By twisting of the nanowire structure, the helical arrangement allows the atoms to pack closer, improving the quality of bonding for the surface atoms.

To visualize the atoms with different coordination number, they are marked with colors in the hexagonal nanowire and the multi-shell FCC (Fig. 4C). The capping atoms at both ends are removed for clarity. In hexagonal nanowire, it can be seen that the surface atoms have in general lower coordination number (7 and 8), with the lowest (5) at the edge of the hexagonal nanowire. In contrast, the atoms in the inner layers mostly have coordination number exceeding 10. For the multi-shell_FCC, the outer shell is consisted of 7- and 8-coordination atoms, and the inner shells have atoms with coordination number surpassing 9. Therefore, the transition from the 5-coordination surface atoms to the 7- and 8-coordination atoms should contribute mainly to the differences of

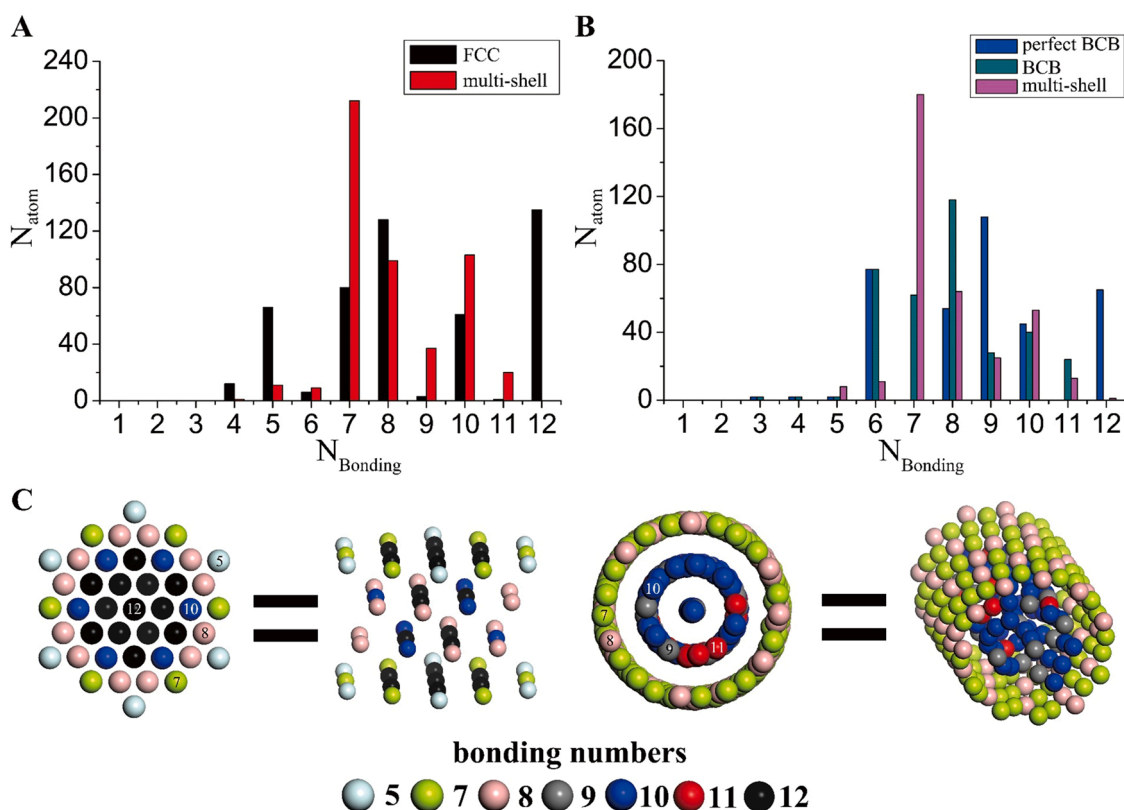


Fig. 4. Histograms showing the distribution of atoms with different coordination number numbers: A) in FCC and the multi-shell structure transformed from FCC; B) in perfect BCB, relaxed BCB and the incomplete multi-shell structure transformed from BCB. (C) Positions of the atoms with different coordination number numbers in FCC and the multi-shell structure. Atoms are distinguished through different colors. (For interpretation of the references to colour in this figure legend, the reader is referred to the web version of this article.)

energies between the two structures.

For the transformation of BCB nanowire, the average coordination number for the perfect BCB, the optimized initial BCB, and the multi-shell-like final structure are 8.79, 7.83 and 7.85, whereas the average bonding lengths are 2.97 Å, 2.88 Å, and 2.87 Å, respectively (Table 1). Same as the above arguments, the ideal BCB structure is the extreme case where the higher average coordination number leads to the lowest stability. For the latter two nanowires, while the differences in the average numbers are small, the breakdown reveals more information: the initial optimization weakens the internal atoms, diminishing the atoms with 12 bonds and mainly increasing the 7- and 8-coordination atoms. Upon further transformation, the 7-, 8-, and 10-coordination atoms become the dominant groups in the structure.

To obtain the interaction energy between each atom and nanowire, the atoms in the hexagonal nanowire is categorized according their coordination number and location (Table 2). We calculated separately the energies of the overall nanowire, each category of atoms in one row, and the nanowire without the atoms. Hence, subtraction of the latter two items from the first one gives the interaction energy.

The nanowire with diameter of 11.79 Å is first studied. There is a general increase of interaction with the increase of coordination number from 5 to 10. Among them, the 5-coordination atoms are by far the most unstable (−17.67 eV), suggesting their prominent role. Unexpectedly, the 12-coordination atoms exhibit similar interaction to the 10-coordination atoms, possibly because the 10-coordination atom locates near the outer boundary, in bonding with the low-coordination atoms (7- and 8-coordination atoms, Fig. 4C). The single row 12-coordination atom at the center of nanowire comes out with the largest interaction (−23.28 eV) than its surrounding neighbors.

Then, nanowires with different diameters are constructed for comparison. The nanowires with diameter of 17.30 and 23.07 Å present the

Table 2

Interaction energies of atoms with different coordination number in nanowires. Atom with same coordination number under different environment are calculated respectively. Nanowires with different diameters are considered as comparison.

Coordination number	11.79 Energies(eV)	Diameters (Å)	
		17.30	23.07
5	− 17.67	− 17.70	− 17.74
7	− 19.34	− 19.76	− 20.22
8	− 20.93	− 20.35	− 20.58
	− 20.46		
10	− 21.97	− 21.23	− 21.27
	− 22.05		
12	− 23.28	− 19.88	− 19.78
	− 21.26	− 20.11	− 19.79
	− 21.45	− 19.41	− 19.35
	− 21.54	− 20.08	− 20.13
			− 19.61

same trend when coordination number increases from 5 to 10, but the 12-coordination atoms come up with a weaker interaction than the 10-coordination atoms (by about 1 eV). Judging from the values, as the 10-coordination atoms near the boundary actually have similar energies, the reversal of interaction should be attributed to the 12-coordination atoms in the inner layers have weaker interaction (by about 1 eV) with the increase of nanowire diameter. Unlike the previous case, the central 12-coordination atom has almost the same energy as its neighbors.

The interaction energies clearly show that the low-coordination surface atoms have much weaker interactions than the normal 12-

coordination atoms (by 2–5 eV), hence supporting our hypothesis that the change of surface atoms is the critical factor in transformation. With the increase of nanowire diameter, the surface atoms have basically unchanged interactions, whereas the 12-coordination atoms in the inner layers become slightly weaker. After the nanowire transformation, the 5-coordination atoms turned into the 7-coordination atoms, whereas the 12-coordination atoms became the 9-, 10-, and 11-coordination atoms (Fig. 4A). Table 2 shows that the former has a much larger energy difference (1.67 eV) than the latter (about 0.13 eV on average for 10- and 12-coordination atoms). It should be noted that the nanowire diameter is an important factor for the driving force: The proportion of the surface atoms would decrease continuously with the increase of nanowire diameter, so that the energy difference mentioned above would be inadequate to drive the transformation of thicker nanowires.

3.5. The generation of twisting

In this part, we would first focus on the atomic motion during the transformation. Then, the trigger of bending is explored. At last, the relationship between bending and twisting is discussed.

Previously, twisting is proven in the transformation from the pre-

synthesized straight nanowires to the twisted double helices and braided nanoropes [6,8]. To evaluate the extent of twisting, the detailed atomic motion during the transformation to helix is taken into consideration. The center axis of nanowire is set as the base line to measure the rotation of atoms (see details in Methods). We first figure out the rotation angle of each atom in a trajectory and the extent of rotation is represented by the gradient of color along the nanowire (Fig. 5A). The atoms at the left ends come up with evident counterclockwise rotation (red blocks), those at the right ends come up with clockwise rotation (blue blocks), and the atoms in the middle are more random without a clear trend. Further analysis of 8 trajectories showed basically the same trend. Hence, the process can be best described as a twisting towards the opposite direction from both ends.

In addition to the atomic rotation around the nanowire axis, there are multiple bending motions during the lattice transformation (Fig. 5B). Here, bending is defined as the relative movements of the nanowire segments that cause the nanowire to deviate from a straight line. From the atomic movements extracted from the simulation, the reorganization can be categorized into two steps: First, there is a slight slip along the close-packed planes, as illustrated by the slip of the left- and right-most layers. Then, atoms nearby would accumulate at the

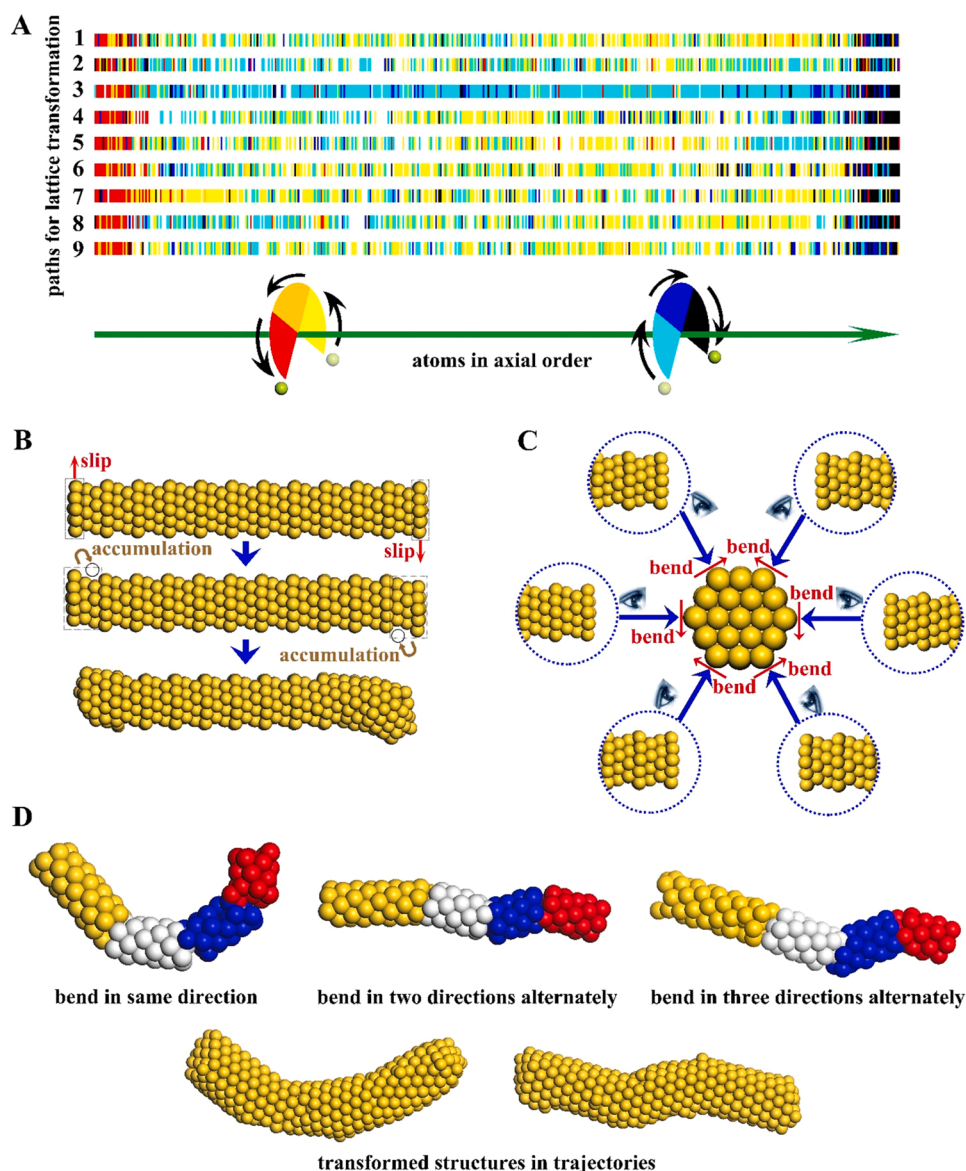


Fig. 5. (A) Diagram illustrating the 9 trajectories, where the rotation angles are represented by the color gradient: red for counterclockwise rotation, and blue for clockwise. Each block represents an atom, arranged in the order of their numeric sequence along the axis of the nanowire. The center axis of nanowire is set as the base line to measure the rotation of atoms. (B) Schematics illustrating the collective slip movement of atoms in a layer and the surface migration of individual atoms. Their combination leads to bends of nanowire with specific structure. (C) Schematics illustrating the 3 possible bending directions for hexagonal nanowire. (D) Manipulating the bending direction of segments arbitrarily through three modes: bending to the same direction, bending to two directions alternately, and bending to three directions alternately. The transformed structures in the trajectories are given as contrasts. (For interpretation of the references to colour in this figure legend, the reader is referred to the web version of this article.)

concave region indicated in Fig. 5B via surface migration. Combination of such motions eventually causes the nanowire to bend, and simultaneously improving the bonding of the surface atoms. In other words, the slipping is the 1st-order collective motions of atoms in a layer, whereas the surface migration of atoms becomes the 2nd-order fix of the structure, both are driven by the energy minimization towards the multi-shell structure. In the process, the slipping and migration are the actual pathways of dislocating the atoms to different layers. In a word, the combination of movements shown in Fig. 5B would result in the bending to the specific direction (The progress could be found in [movie S1](#)).

Supplementary material related to this article can be found online at [doi:10.1016/j.mtcomm.2022.104319](https://doi.org/10.1016/j.mtcomm.2022.104319).

For hexagonal nanowire, there are 6 possible bending directions on the basis of the above analysis, and it becomes 3 when considering the symmetry (Fig. 5C, the possible bending directions are marked with red arrows). To understand the relationship between the bending and the helix transformed from the Au nanowire, we arbitrarily manipulate the bending of a straight nanowire (Fig. 5D): The 4 segments are either bent to the same direction; or bent in two directions alternately; or bent in three directions alternately. Judging from the morphology of the products in different trajectories, it is the combination of bending in different directions that result in the twisting of nanowire (The progress of twisting could be found in [movie S2-6](#)). As most of the trajectories lead to random bending in all three directions, additional chirality control is necessary to achieve a coherent chirality in all trajectories.

Supplementary material related to this article can be found online at [doi:10.1016/j.mtcomm.2022.104319](https://doi.org/10.1016/j.mtcomm.2022.104319).

4. Conclusions

In summary, using the SSW global optimization method to search for possible transformations of Au nanowires, we show that Au nanowire with FCC lattice could transform into a helix with multi-shell atomic structure spontaneously. Compared with former investigations on nanowires, we realize the twisting of nanowires, and investigate such mechanical motion with theoretical calculation for the first time. As a consequence, the mechanism of nanowire's twisting in nanoscale could be revealed. Morphologies of nanowires would affect the routes of transformation, often leading to trapped meta-stable states, but they are overall moving towards the multi-shell atomic structure. Such characteristic transformations have not been reported previously, which reveals unique structures in nanoscale. The process is driven by the surface atoms seeking improved bonding (with smoother surface), at the cost of the internal atoms. Bending is achieved by a combination of collective slip movement and the surface migration of individual atoms. The bending in the different sections of nanowire results in the overall twisting of nanowire.

CRediT authorship contribution statement

Guangyu He (First Author): Conceptualization, Methodology, Software, Investigation, Formal analysis, Writing – original draft. **Ruoxu Wang:** Data curation, Writing – original draft. **Jie Fan:** Writing – review & editing. **Shi Liu:** Writing – review & editing. **Hongyu Chen (Corresponding author):** Conceptualization, Funding acquisition, Resources, Supervision, Writing – review & editing.

Declaration of Competing Interest

The authors declare that they have no known competing financial interests or personal relationships that could have appeared to influence the work reported in this paper.

Data Availability

I have shared the link to my data/code at the Attach File step.

Acknowledgements

This work is financially supported by the National Natural Science Foundation of China (91956109) and the Foundation of Westlake University. The authors are very grateful for the assistance with Profs. Zhipan Liu and Cheng Shang on the performing LASP software in the training of NN potential.

Appendix A. Supporting information

Supplementary data associated with this article can be found in the online version at [doi:10.1016/j.mtcomm.2022.104319](https://doi.org/10.1016/j.mtcomm.2022.104319).

References

- [1] S. Bianchini, A. Lage, T. Siu, T. Shinbrot, E. Altschuler, Upstream contamination by floating particles, *Proc. R. Soc. A: Math. Phys. Eng. Sci.* 469 (2157) (2013).
- [2] M. Medina-Sanchez, L. Schwarz, A.K. Meyer, F. Hebenstreit, O.G. Schmidt, Cellular cargo delivery: toward assisted fertilization by sperm-carrying micromotors, *Nano Lett.* 16 (1) (2016) 555–561.
- [3] L. Chen, H. Wang, J. Xu, X. Shen, L. Yao, L. Zhu, Z. Zeng, H. Zhang, H. Chen, Controllable reversible elastic deformation of carbon nanotube rings, *J. Am. Chem. Soc.* 133 (25) (2011) 9654–9657.
- [4] L. Chen, S. Yu, H. Wang, J. Xu, C. Liu, W.H. Chong, H. Chen, General methodology of using oil-in-water and water-in-oil emulsions for coiling nanofilaments, *J. Am. Chem. Soc.* 135 (2) (2013) 835–843.
- [5] J. Xu, H. Wang, C. Liu, Y. Yang, T. Chen, Y. Wang, F. Wang, X. Liu, B. Xing, H. Chen, Mechanical nanosprings: induced coiling and uncoiling of ultrathin Au nanowires, *J. Am. Chem. Soc.* 132 (34) (2010) 11920–11922.
- [6] Y. Lu, S. Yang, J. Xu, Z. Liu, H. Wang, M. Lin, Y. Wang, H. Chen, Twisting ultrathin Au nanowires into double helices, *Small* 14 (34) (2018), e1801925.
- [7] Y. Wang, Q. Wang, H. Sun, W. Zhang, G. Chen, Y. Wang, X. Shen, Y. Han, X. Lu, H. Chen, Chiral transformation: from single nanowire to double helix, *J. Am. Chem. Soc.* 133 (50) (2011) 20060–20063.
- [8] Y. Lu, X. Cheng, H. Li, J. Zhao, W. Wang, Y. Wang, H. Chen, Braiding ultrathin Au nanowires into ropes, *J. Am. Chem. Soc.* 142 (24) (2020) 10629–10633.
- [9] L.H. Wang, Y. Zhang, Z. Zeng, H. Zhou, J. He, P. Liu, M.W. Chen, J. Han, D. J. Srolovitz, J. Teng, Y.Z. Guo, G. Yang, D.L. Kong, E. Ma, Y.L. Hu, B.C. Yin, X. X. Huang, Z. Zhang, T. Zhu, X.D. Han, Tracking the sliding of grain boundaries at the atomic scale, *Science* 375 (6586) (2022) 1261.
- [10] S. Sun, D. Li, C. Yang, L. Fu, D. Kong, Y. Lu, Y. Guo, D. Liu, P. Guan, Z. Zhang, J. Chen, W. Ming, L. Wang, X. Han, Direct atomic-scale observation of ultrasmall Ag nanowires that exhibit fcc, bcc, and hcp structures under bending, *Phys. Rev. Lett.* 128 (1) (2022), 015701.
- [11] J. Diao, K. Gall, M.L. Dunn, Surface-stress-induced phase transformation in metal nanowires, *Nat. Mater.* 2 (10) (2003) 656–660.
- [12] J. Diao, K. Gall, M. Dunn, Surface stress driven reorientation of gold nanowires, *Phys. Rev. B* 70 (7) (2004).
- [13] Park, S.J.N.L. Harold, Stress-induced martensitic phase transformation in intermetallic nickel aluminum nanowires, *Nano Lett.* 6 (5) (2006) 958–962.
- [14] W. Liang, M. Zhou, F. Ke, Shape memory effect in Cu nanowires, *Nano Lett.* 5 (10) (2005) 2039–2043.
- [15] W. Liang, M. Zhou, Pseudoelasticity of single crystalline Cu nanowires through reversible lattice reorientations, *J. Eng. Mater. Technol.* 127 (4) (2005) 423–433.
- [16] H.S. Park, K. Gall, J.A. Zimmerman, Shape memory and pseudoelasticity in metal nanowires, *Phys. Rev. Lett.* 95 (25) (2005), 255504.
- [17] O. Gülseren, F. Ercolessi, E. Tosatti, Non-crystalline structures of ultra-thin unsupported nanowires, *Phys. Rev. Lett.* 80 (17) (1998) 3775–3778.
- [18] S.D. Huang, C. Shang, P.L. Kang, X.J. Zhang, Z.P. Liu, LASP: Fast global potential energy surface exploration, *WILEY Interdiscip. Rev.-Comput. Mol. Sci.* 9 (6) (2019).
- [19] S.D. Huang, C. Shang, X.J. Zhang, Z.P. Liu, Material discovery by combining stochastic surface walking global optimization with a neural network, *Chem. Sci.* 8 (9) (2017) 6327–6337.
- [20] C. Shang, Z.P. Liu, Stochastic surface walking method for structure prediction and pathway searching, *J. Chem. Theory Comput.* 9 (3) (2013) 1838–1845.
- [21] J. Behler, M. Parrinello, Generalized neural-network representation of high-dimensional potential-energy surfaces, *Phys. Rev. Lett.* 98 (14) (2007).
- [22] S.D. Huang, C. Shang, P.L. Kang, Z.P. Liu, Atomic structure of boron resolved using machine learning and global sampling, *Chem. Sci.* 9 (46) (2018) 8644–8655.
- [23] S. Ma, S.-D. Huang, Z.-P. Liu, Dynamic coordination of cations and catalytic selectivity on zinc-chromium oxide alloys during syngas conversion, *Nat. Catal.* 2 (8) (2019) 671–677.
- [24] P.L. Kang, C. Shang, Z.P. Liu, Glucose to 5-Hydroxymethylfurfural: origin of site-selectivity resolved by machine learning based reaction sampling, *J. Am. Chem. Soc.* 141 (51) (2019) 20525–20536.
- [25] G.K. A, J. Furthmüller, Efficiency of ab-initio total energy calculations for metals and semiconductors using a plane-wave basis set, *Comput. Mater. Sci.* 6 (1) (1996) 15–50.
- [26] J. Perdew, K. Burke, M. Ernzerhof, Generalized gradient approximation made simple, *Phys. Rev. Lett.* 78 (7) (1996) 1396.

- [27] G. Kresse, D. Joubert, From ultrasoft pseudopotentials to the projector augmented-wave method, *Phys. Rev. B* 59 (3) (1999) 1758–1775.
- [28] H.J.P. Monkhorst, Special points for Brillouin-zone integrations, *Phys. Rev. B* 13 (12) (1976) 5188–5192.
- [29] P. Giannozzi, S. Baroni, N. Bonini, M. Calandra, R. Car, C. Cavazzoni, D. Ceresoli, G.L. Chiarotti, M. Cococcioni, I. Dabo, A. Dal Corso, S. de Gironcoli, S. Fabris, G. Fratesi, R. Gebauer, U. Gerstmann, C. Gougoussis, A. Kokalj, M. Lazzeri, L. Martin-Samos, N. Marzari, F. Mauri, R. Mazzarello, S. Paolini, A. Pasquarello, L. Paulatto, C. Sbraccia, S. Scandolo, G. Sclauzero, A.P. Seitsonen, A. Smogunov, P. Umari, R.M. Wentzcovitch, QUANTUM ESPRESSO: a modular and open-source software project for quantum simulations of materials, *J. Phys. Condens Matter* 21 (39) (2009), 395502.
- [30] X.J. Zhang, C. Shang, Z.P. Liu, Double-ended surface walking method for pathway building and transition state location of complex reactions, *J. Chem. Theory Comput.* 9 (12) (2013) 5745–5753.
- [31] J.D. Bernal, Geometry of the structure of monatomic liquids, *Nature* 185 (4706) (1960) 68–70.
- [32] A.H. Boerdijk, Some remarks concerning close-packing of equal spheres, *Philips Res. Rep.* 7 (4) (1952) 303–313.
- [33] J.J. Velazquez-Salazar, R. Esparza, S.J. Mejia-Rosales, R. Estrada-Salas, A. Ponce, F. L. Deepak, C. Castro-Guerrero, M. Jose-Yacaman, Experimental evidence of icosahedral and decahedral packing in one-dimensional nanostructures, *ACS Nano* 5 (8) (2011) 6272–6278.
- [34] J. Han, L. Fang, J. Sun, Y. Han, K. Sun, Length-dependent mechanical properties of gold nanowires, *J. Appl. Phys.* 112 (11) (2012), 114314.
- [35] Y.-H. Wen, Y. Zhang, Q. Wang, J.-C. Zheng, Z.-Z. Zhu, Orientation-dependent mechanical properties of Au nanowires under uniaxial loading, *Comput. Mater. Sci.* 48 (3) (2010) 513–519.
- [36] Y. Kondo, K. Takayanagi, Synthesis and characterization of helical multi-shell gold nanowires, *Science* 289 (5479) (2000) 606–608.
- [37] Y. Zhu, J. He, C. Shang, X. Miao, J. Huang, Z. Liu, H. Chen, Y. Han, Chiral gold nanowires with Boerdijk-Coxeter-Bernal structure, *J. Am. Chem. Soc.* 136 (36) (2014) 12746–12752.